

# LeTO: Learning Constrained Visuomotor Policy with Differentiable Trajectory Optimization

Zhengtong Xu, Yu She\*

**Abstract**—This paper introduces LeTO, a method for learning constrained visuomotor policy via differentiable trajectory optimization. Our approach integrates a differentiable optimization layer into the neural network. By formulating the optimization layer as a trajectory optimization problem, we enable the model to end-to-end generate actions in a safe and constraint-controlled fashion without extra modules. Our method allows for the introduction of constraints information during the training process, thereby balancing the training objectives of satisfying constraints, smoothing the trajectories, and minimizing errors with demonstrations. This “gray box” method marries the optimization-based safety and interpretability with the powerful representational abilities of neural networks. We quantitatively evaluate LeTO in simulation and on the real robot. In simulation, LeTO achieves a success rate comparable to state-of-the-art imitation learning methods, but the generated trajectories are of less uncertainty, higher quality, and smoother. In real-world experiments, we deployed LeTO to handle constraints-critical tasks. The results show the effectiveness of LeTO comparing with state-of-the-art imitation learning approaches. We release our code at <https://github.com/ZhengtongXu/LeTO>.

**Index Terms**—Robotic manipulation, imitation learning, differentiable optimization.

## I. INTRODUCTION

Imitation learning [1] focuses on deriving robot policies from demonstrations. This process can be formulated as a supervised learning task, aiming to learn the mapping between observations and robot actions. Through imitation learning, robots can perform highly complex and diverse tasks [2]–[8].

However, ensuring the safety of robots is very important due to the interaction between robots and the real world. In contrast to optimization-based trajectory generation methods, imitation learning often exhibits greater uncertainty, which can lead to system instability, reduced robustness, and safety concerns. Hence, in comparison to other supervised learning problems, this pose novel and exceptional challenges in safety for imitation learning.

Existing works focus on different aspects and challenges of imitation learning, such as improving action accuracy by addressing compounding errors [4] and represent multi-modal distributions by implicit policy [2], [9], [10]. However, these methods overlook the critical aspects of safety and smoothness of generated trajectories. For robotic systems, their behaviors need to meet specific constraints to ensure the safety of the system. Moreover, for certain tasks, the

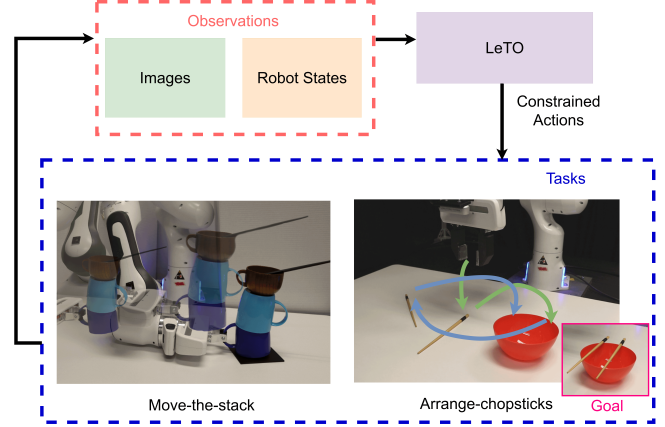


Fig. 1: In LeTO, we enable the model to end-to-end generate actions in a safe and constraint-controlled fashion without extra modules. To the best of our knowledge, LeTO is the first visuomotor imitation learning framework that not only utilizes differentiable optimization but also demonstrates its efficacy in real-world robotic manipulation tasks.

robot actions also need to meet specific constraints to ensure their successful completion. In addition, adding explainable constraints for neural network-based algorithms, often called “black boxes”, is much harder than for traditional model-based methods.

In this paper, we propose LeTO, learning constrained visuomotor policy with differentiable trajectory optimization. The strengths and novelties of our method are as follows.

1) **Differentiable optimization layer:** We integrate a differentiable optimization layer to the neural network and formulate it as a trajectory optimization problem. We demonstrate that the differentiable optimization layer we design has optimization feasibility during training and model representation capability. To the best of our knowledge, our work is the first visuomotor imitation learning framework that not only utilizes differentiable optimization but also demonstrates its efficacy in both simulation and real-world robotic manipulation tasks.

2) **Safe and constrained action generation:** In our approach, we formulate the optimization layer as a trajectory optimization problem. Through this approach, the policy generate constrained trajectories, enhancing the overall safety and smoothness of robot actions. Since the model incorporates position, velocity, and acceleration constraints during end-to-end training, it ensures robot safety without compromising performance when deploying the model as a real-time policy. Compared to the “black box” characteristics of neural networks, our approach can be described as a

\*Address all correspondence to this author.

Zhengtong Xu and Yu She are with the School of Industrial Engineering, Purdue University, West Lafayette, USA (E-mail: {xu1703, shey}@purdue.edu).

“gray box” that combines the safety and interpretability of optimization-based trajectory generation with the powerful representational capabilities of neural networks.

We evaluate LeTO both in simulations (Section IV) and on real robot tasks (Section V) quantitatively, and benchmark with diffusion policy [11], LSTM-GMM [12], and IBC [10]. In the simulated tests, LeTO achieves a success rate comparable to diffusion policy and better than LSTM-GMM and IBC, but the generated trajectories are of less uncertainty, higher quality, and smoother comparing with these methods. On the real robot, we implement constraints-critical manipulation tasks using LeTO, which highlights LeTO’s strengths.

## II. RELATED WORK

### A. Trajectory Optimization

Trajectory optimization is pivotal in generating safe and smooth trajectories for robots and remains an active area of research. CHOMP [13] approaches trajectory optimization by gradient techniques, focusing on optimizing the trade-off between safety and smoothness. TrajOpt [14] uses a sequential convex optimization to generate smooth and collision-free trajectories and can use naive straight-line initializations that might be in collision. The minimum-snap trajectory optimization [15] uses piecewise polynomials to represent the trajectory and is optimized by quadratic programs. The work in [16] proposes a method for reformulating nondifferentiable collision avoidance constraints into smooth, differentiable constraints and enables real-time optimization-based trajectory planning.

In LeTO, we innovatively combine trajectory optimization with imitation learning by differentiable optimization, to generate smooth and constraint-compliant trajectories during policy rollout. Our model is trained end-to-end. During the training process, LeTO not only learns the policy from human demonstrations but also learns the appropriate trajectory optimization parameters suitable for the policy.

### B. Imitation Learning

The basic way of imitation learning explicitly maps observations to actions [1], [17]–[21]. It can be trained using a regression loss. However, these policies are not ideal for capturing multi-modal distributions [10].

Prior works have aimed to represent multi-modal distributions by converting the regression into classification [22]–[24], using action discretization coupled with a multi-task action correction [25], using MDNs [12], and using implicit modeling that including energy-based model [9], [10] and diffusion model [2]. However, these methods overlook the critical aspects of safety for robot systems. For robotic systems, their behaviors need to meet specific constraints to ensure the safety of the system and the successful completion of tasks.

LeTO focuses on combining explainable and model-based trajectory optimization with imitation learning. In this way, LeTO can be end-to-end trained and generate action in a safe and constraint-controlled fashion without extra modules.

### C. Differentiable Optimization in Robot Learning

Previous works utilize differentiable optimization for modeling discontinuous functions and dynamics [26], [27]. Additionally, some works focus on combining model-based methods with neural networks through differentiable optimization, such as using differentiable MPC [28] and koopman operator [29]. However, these methods are not suitable for tasks with high-dimensional observations, such as using camera images from multiple viewpoints.

The work in [30] proposes a tactile-reactive grasping controller that combines image encoder and differentiable MPC. However, it can not be used for more general policy learning.

For robot navigation and obstacle avoidance, various end-to-end learning frameworks embed with differentiable optimization are proposed, such as using control barrier function [31], gradient-based correction [32], and stacking prediction, planning, and control in a differentiable way [33]. However, all these methods are not suited for performing manipulation tasks.

DiffTOP [34] is a method that integrate differentiable trajectory optimization as the policy representation to generate actions. In integrating imitation learning, DiffTOP focuses on capturing multi-modal distributions. However, it can not generating safe and constrained trajectories. In contrast, LeTO focuses on how the integration of differentiable trajectory optimization into the imitation learning framework enables the generation of trajectories that not only perform tasks effectively but also satisfy constraints.

Another category of methods closely related to LeTO is riemannian motion policy (RMP) [35] and its extensions [36], [37]. Specifically, the works in [36], [37] enhance RMP’s integration into end-to-end robot learning by incorporating automatic differentiation. This enables end-to-end training and inference for policies with RMP structures. Methods based on RMP are particularly focused on generating motion in spaces with high degrees of freedom and nonlinear dynamics. In contrast, LeTO offers a capable form of generating constrained motion at the task space trajectory level with differentiable optimization. This advantage makes it better suited for adaptation to visuomotor policies and demonstrates superior performance in real tasks. To the best of our knowledge, our work is the first visuomotor imitation learning framework that not only utilizes differentiable optimization but also demonstrates its efficacy in both simulation and real-world robotic manipulation tasks.

## III. APPROACH

In this paper, we assume access to an offline trajectories dataset of the task we want to do. The goal is to learn a policy from this dataset offline and can successfully do the task by running the policy online. The overview of LeTO is shown in Fig. 2. In this section, we will detail the design of the model.

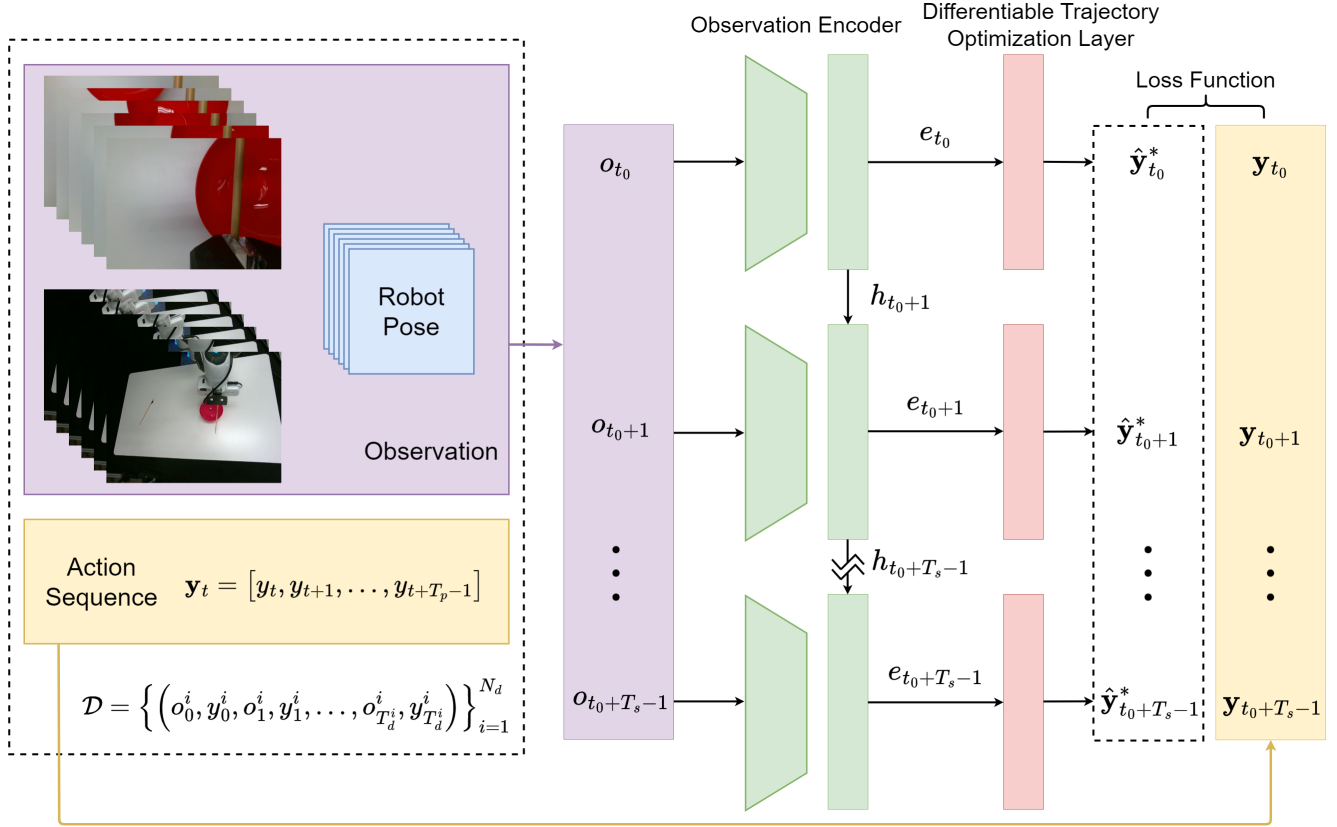


Fig. 2: Overview of LeTO. We enable the model to end-to-end generate actions in a safe and constraint-controlled fashion by integrating a differentiable trajectory optimization layer.

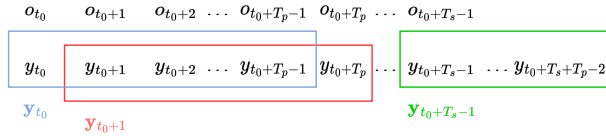


Fig. 3: Illustration of training data sampling.

### A. Training Data Sampling

In this paper, we categorize actions into two types: one is discrete actions, such as grasping and releasing; the other is continuous actions, such as the motion of the robot. For continuous actions, we consider the velocity/increment of the end-effector as the action [12], [17], [18], [25], [38], [39]. Denote the dataset as

$$\mathcal{D} = \left\{ \left( o_0^i, y_0^i, o_1^i, y_1^i, \dots, o_{T_d}^i, y_{T_d}^i \right) \right\}_{i=1}^{N_d},$$

where  $o$  represents the observations of the robot, such as images of the cameras with different views and robot states and  $y \in \mathbb{R}^{D_y}$  represents the demonstrated action aligned with the observation  $o$ .  $N_d$  is the total number of the demonstrated trajectories,  $T_d$  is the total length of a trajectory, and  $D_y$  is the dimension of action  $y$ .

Inspired by model predictive control and diffusion policy [2], in LeTO, we predict a action sequence at every time step. Moreover, we care about how to predict trajectories that satisfy constraints rather than action sequences simply

fitting the human demonstration. Therefore, before training, we first sample many fixed-length sequences in following format from the dataset

$$\left( o_{t_0}, \mathbf{y}_{t_0}, o_{t_0+1}, \mathbf{y}_{t_0+1}, \dots, o_{t_0+T_s-1}, \mathbf{y}_{t_0+T_s-1} \right),$$

where  $\mathbf{y}_t = \left[ y_t^T, y_{t+1}^T, \dots, y_{t+T_p-1}^T \right]^T \in \mathbb{R}^{T_p D_y}$ .  $T_s$  is the length of each data sampling and  $T_p$  is the length of the predicted action sequence, as shown in Fig. 3. The learning objective is minimizing the errors between the predicted  $\hat{\mathbf{y}}_t^*$  and  $\mathbf{y}_t$  (e.g. using MSE loss to assess the distance between them), as shown in Fig. 2. During policy rollout, the robot will execute the first  $T_a$ -step actions of  $\hat{\mathbf{y}}_t^*$ , and then repeat the same process based on new observations. This process is typically called receding horizon planning/control.

Continuous actions need to be constrained to ensure actions safety and smoothness while discrete actions do not. Therefore, we define a selection matrix  $S$  to pick the continuous action vector  $v$  that require to be constrained.

$$v = S y \in \mathbb{R}^{D_v}. \quad (1)$$

As mentioned earlier, we focus on a velocity-based action space, so here,  $v$  refers to the velocity at which the robot is being controlled and  $D_v$  is the dimension of  $v$ .

### B. Observation Encoder

The observation encoder maps the observations, like raw RGB images and robot states, into a latent embedding  $e$  and

is trained end-to-end with LeTO. To capture the sequential correlation of the task, we use a recurrent neural network (RNN) architecture,  $E_\theta$ , where the right subscript  $\theta$  represent the parameters of the network. We choose long short-term memory (LSTM) as our RNN model. At each time step,  $e_t, h_{t+1} = E_\theta(o_t, h_t)$ , where  $h$  is the hidden state. We define  $e_t \in \mathbb{R}^{T_p D_y}$ . More detailed reasons of setting the dimension as  $T_p D_y$  can be seen at Section III-C.

### C. Differentiable Trajectory Optimization Layer

The differentiable trajectory optimization (DTO) layer maps the embedding  $e_t$  to a predicted action sequence  $\hat{\mathbf{y}}_t = [\hat{y}_t^T, \hat{y}_{t+1}^T, \dots, \hat{y}_{t+T_p-1}^T]^T \in \mathbb{R}^{T_p D_y}$ . In this section, we will show how to design this layer based on trajectory optimization, learn this layer during training, and integrate it with the whole neural network.

By equation (1), the predicted velocity command sequence

$$\hat{\mathbf{v}}_t = \mathbf{S}\hat{\mathbf{y}}_t = [\hat{v}_{t+1}^T, \hat{v}_{t+2}^T, \dots, \hat{v}_{t+T_p-1}^T]^T \in \mathbb{R}^{T_p D_v}, \quad (2)$$

where  $\mathbf{S} = \text{blkdiag}(S, \dots, S) \in \mathbb{R}^{T_p D_v \times T_p D_y}$ . Then the predicted acceleration sequence and position sequence are

$$\begin{aligned} \hat{\mathbf{a}}_t &= [\hat{a}_t^T, \hat{a}_{t+1}^T, \dots, \hat{a}_{t+T_p-2}^T]^T \\ &= \frac{1}{\Delta t} [\hat{v}_{t+1}^T - \hat{v}_t^T, \dots, \hat{v}_{t+T_p-1}^T - \hat{v}_{t+T_p-2}^T]^T \\ &= \frac{1}{\Delta t} \begin{bmatrix} -1 & 1 & & & \\ & -1 & 1 & & \\ & & & \ddots & \\ & & & & -1 & 1 \end{bmatrix} \hat{\mathbf{v}}_t \\ &= \mathbf{A}_{\text{diff}} \hat{\mathbf{v}}_t \in \mathbb{R}^{T_p D_v - D_v}, \\ \hat{\mathbf{p}}_t &= [\hat{p}_{t+1}, \dots, \hat{p}_{t+T_p-1}]^T \\ &= \begin{bmatrix} p_t \\ p_t \\ \vdots \\ p_t \end{bmatrix} + \begin{bmatrix} \Delta t & & & \\ \Delta t & \Delta t & & \\ \vdots & \vdots & \ddots & \\ \Delta t & \Delta t & \dots & \Delta t \end{bmatrix} \hat{\mathbf{v}}_t \\ &= \mathbf{p}_{t,0} + \mathbf{A}_{\text{inte}} \hat{\mathbf{v}}_t \in \mathbb{R}^{T_p D_v - D_v}, \end{aligned} \quad (3)$$

where  $\hat{p}_{t+i} = p_t + \hat{v}_t \Delta t + \dots + \hat{v}_{t+i-1} \Delta t, i = 1, \dots, T_p - 1$ , and  $p_t$  is the robot end-effector position at time step  $t$ .

The sequence  $\hat{\mathbf{p}}_t, \hat{\mathbf{v}}_t$ , and  $\hat{\mathbf{a}}_t$  together constitute the trajectory generated by the policy. To optimize the trajectory, we must consider the relationship between  $\hat{\mathbf{p}}_t, \hat{\mathbf{v}}_t$ , and  $\hat{\mathbf{a}}_t$  and human demonstration, as well as the constraints of  $\hat{\mathbf{p}}_t, \hat{\mathbf{v}}_t$ , and  $\hat{\mathbf{a}}_t$ . Based on this, the forward pass of the DTO layer is the following optimization problem:

$$\hat{\mathbf{y}}_t^* = \underset{\hat{\mathbf{y}}_t}{\text{argmin}} \frac{1}{2} \hat{\mathbf{y}}_t^T \mathbf{Q} \hat{\mathbf{y}}_t + e_t^T \hat{\mathbf{y}}_t + \frac{\alpha}{2} \hat{\mathbf{a}}_t^T \hat{\mathbf{a}}_t, \quad (5)$$

$$\begin{aligned} \text{subject to } & b_{\min} \leq A_{\text{pos}} \hat{p}_{t+i} \leq b_{\max}, i = 1, \dots, T_p - 1, \\ & v_{\min} \leq \hat{v}_{t+j} \leq v_{\max}, j = 0, \dots, T_p - 1, \\ & a_{\min} \leq \hat{a}_{t+k} \leq a_{\max}, k = 0, \dots, T_p - 2. \end{aligned}$$

Rewrite the optimization problem (5) by equations (2), (3), and (4), then we have

$$\hat{\mathbf{y}}_t^* = \underset{\hat{\mathbf{y}}_t}{\text{argmin}} \frac{1}{2} \hat{\mathbf{y}}_t^T \bar{\mathbf{Q}} \hat{\mathbf{y}}_t + e_t^T \hat{\mathbf{y}}_t, \quad (6)$$

subject to

$$\mathbf{b}_{\min} \leq \mathbf{A}_{\text{pos}}(\mathbf{p}_{t,0} + \mathbf{A}_{\text{inte}} \mathbf{S} \hat{\mathbf{y}}_t) \leq \mathbf{b}_{\max}, \quad (7)$$

$$\mathbf{v}_{\min} \leq \mathbf{S} \hat{\mathbf{y}}_t \leq \mathbf{v}_{\max}, \quad (8)$$

$$\mathbf{a}_{\min} \leq \mathbf{A}_{\text{diff}} \mathbf{S} \hat{\mathbf{y}}_t \leq \mathbf{a}_{\max}, \quad (9)$$

$$\text{where } \bar{\mathbf{Q}} = (\mathbf{Q} + \alpha \mathbf{S}^T \mathbf{A}_{\text{diff}}^T \mathbf{A}_{\text{diff}} \mathbf{S}),$$

$$\begin{aligned} \mathbf{A}_{\text{pos}} &= \text{blkdiag}(A_{\text{pos}}, \dots, A_{\text{pos}}) \\ &\in \mathbb{R}^{(T_p D_v - D_v) \times (T_p D_v - D_v)}. \end{aligned}$$

The coefficient  $\alpha$  controls the smoothness of the trajectory. It can be observed in (5) that the larger the value of  $\alpha$ , the greater the cost associated with the sum of accelerations, leading the optimization problem to generate trajectories with a smaller sum of accelerations.  $A_{\text{pos}}$  and  $b_{\max, \min}$  define the convex constraints that the position must satisfy.  $v_{\max, \min}$  and  $a_{\max, \min}$  define the constraints for the velocity and acceleration of the trajectory.  $\alpha, A_{\text{pos}}, b_{\max, \min}, v_{\max, \min}$  and  $a_{\max, \min}$  are interpretable and model-based, so we do not need to learn these parameters during training. Instead, it is advisable to specify them according to the requirements of the task. On the contrary,  $\mathbf{Q} \in \mathbb{R}^{T_p D_y}$  is a parameters that we need to learn during training. Next, we will demonstrate how to learn  $\mathbf{Q}$  and its specific meaning in our trajectory optimization problem.

Optimization problem (6) is a quadratic program (QP). Therefore, the layer (6) can perform forward pass and back-propagation in batch form as long as it is always feasible in the training process [40]. The feasibility of (6) can be guaranteed by ensuring  $\mathbf{Q}$  symmetric positive definite [41]. To achieve that, we utilize a Cholesky factorization

$$\mathbf{Q} = \mathbf{L}\mathbf{L}^T + \epsilon \mathbf{I},$$

and directly learn  $\mathbf{L}$ , where  $\mathbf{L}$  is a lower triangular matrix and  $\epsilon$  is a very small scalar (e.g.  $1 \times 10^{-4}$ ). By observing optimization problem (6), Remark 1 can be derived.

**Remark 1** (feasibility of the differentiable optimization layer). *If the constraint  $\mathbf{b}_{\min} \leq \mathbf{A}_{\text{pos}} \mathbf{p}_{t,0} \leq \mathbf{b}_{\max}$  is satisfied at each time step  $t$ , the optimization problem is always feasible, no matter how  $\mathbf{L}$  and  $e_t$  change. This means the optimization problem remains consistently feasible, which ensuring stable training process.  $\mathbf{b}_{\min} \leq \mathbf{A}_{\text{pos}} \mathbf{p}_{t,0} \leq \mathbf{b}_{\max}$  represents that the human demonstrations should satisfy the position constraints. Additionally, the human demonstrations do not need to satisfy the velocity and acceleration constraints strictly, because they have nothing to do with the feasibility of the optimization problem. Further more, for human demonstration, satisfying position constraints is much easier than satisfying the velocity and acceleration constraints.*

Based on that  $\mathbf{Q}$  is symmetric positive definite, the optimization problem (6) can be converted as the following least squares problem:

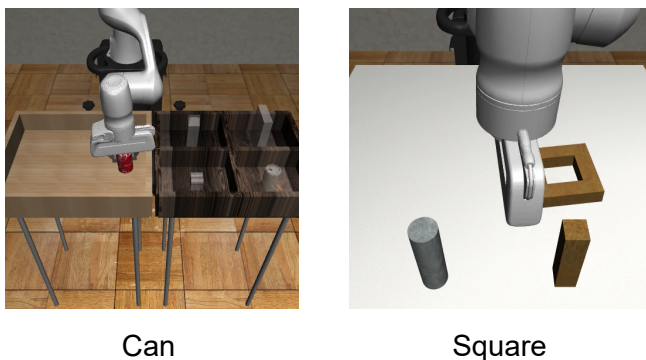


Fig. 4: Simulation benchmarks: pick and place the can (can task) and grasping and assembling the square nut (square task).

$$\hat{\mathbf{y}}_t^* = \underset{\hat{\mathbf{v}}_t}{\operatorname{argmin}} \frac{1}{2} \|\bar{\mathbf{L}}^T \hat{\mathbf{y}}_t - \bar{\mathbf{e}}_t\|^2, \quad (10)$$

subject to (7), (8), and (9),  
 where  $\bar{\mathbf{Q}} = \bar{\mathbf{L}}\bar{\mathbf{L}}^T$ ,  
 $\mathbf{e}_t = -\bar{\mathbf{L}}\bar{\mathbf{e}}_t$ .

Based on Cholesky factorization,  $\bar{\mathbf{L}}$  is a lower triangular matrix with real and positive diagonal entries. By observing optimization problem (10), Remark 2 can be derived.

**Remark 2** (representational power). *DTO layer actually optimize a linear transformation under motion constraints. Since  $\bar{\mathbf{L}}$  is a lower triangular matrix and it is fully ranked, the linear transformation here is*

$$\hat{\mathbf{y}}_t^* = -(\bar{\mathbf{L}}^T)^{-1} \bar{\mathbf{L}}^{-1} \mathbf{e}_t.$$

*Since the observation encoder is just a normal LSTM architecture, it is already has the power of representing the policy. Therefore, the whole model including the DTO layer has the power of fitting the human demonstration.*

#### D. Policy Deployment

When the policy is deployed on the robot, the RNN is unrolled one-step at a time,  $\mathbf{e}_t, h_{t+1} = E_\theta(o_t, h_t)$ . The hidden state  $h$  is refreshed every  $T_s$  steps. In addition, the training is on discrete trajectory clips while the robot trajectory is continuous in reality. Therefore, the forward pass of the DTO layer need to add a new constraint during test time to fully constrain the motion generation.

$$\hat{\mathbf{y}}_t^* = \underset{\hat{\mathbf{y}}_t}{\operatorname{argmin}} \frac{1}{2} \hat{\mathbf{y}}_t^T \bar{\mathbf{Q}} \hat{\mathbf{y}}_t + \mathbf{e}_t^T \hat{\mathbf{y}}_t,$$

subject to (7), (8), and (9),  
 $a_{\min} \Delta t \leq \hat{\mathbf{v}}_t - \hat{\mathbf{v}}_{t-1} \leq a_{\max} \Delta t$

where  $\hat{\mathbf{v}}_{t-1}$  represents the last executed action for the robot at time step  $t$  (executed at time step  $t-1$ ). Adding this new constraint is transferring the model trained on a discrete set of trajectories into continuous online trajectory optimization.

## IV. SIMULATION EVALUATION

We employed two simulation tasks used in [12] for our simulation evaluation: pick and place the can (can task) and grasping and assembling the square nut (square task), as shown in Fig. 4. The results demonstrate that our approach not only achieves success rates comparable to diffusion policy [2], but also significantly surpasses IBC [10] and LSTM+GMM [12]. Furthermore, owing to the presence of constraints and differentiable trajectory optimization, our method exhibits superior performance in terms of generated trajectory quality compared to other methods, which is very important for robot systems.

For training parameters of diffusion policy and LSTM+GMM, we use the default configurations provided in their released code. We also do the same for our realworld evaluation. We have released our code, training data, and checkpoints for reproducing our results.

The can and square tasks are from RoboMimic benchmark [12]. Apart from the most basic lifting task, we opted not to include the tool hanging and transport tasks. As highlighted in [40], solving optimization problems precisely, as we are doing here, exhibits cubic complexity concerning the number of variables and/or constraints. Consequently, our method’s training speed for tasks like tool hanging and transport, which involve large datasets or high dimension outputs, is sluggish, and under limited GPU computational resources, obtaining results within a short time is unfeasible. Nevertheless, as we have already demonstrated the capability of our approach to achieve high successful rates and generate high quality trajectories through the outcomes of the two tasks mentioned above, we decided against further training on the tool hanging and transport tasks.

We train policies on 3 seeds (42, 142, 242), and test in 25 different initial environments for each seeds (totaling 75 conditions). For each task, we train policies on two different types of datasets: Proficient-Human (ph), and Multi-Human (mh) datasets [12]. We report the success rate (see Table I) of all these experiments. We also report metrics for evaluating the quality of the generated trajectories (see Tables II, III, IV, and V).

The velocity action outputs in RoboMimic dataset [12] are normalized to  $[-1, 1]$ . Therefore, for our implementation of LeTO, we impose a normalized velocity constraint  $[-1, 1]$ , and we introduce an acceleration constraint  $[-0.1, 0.1]$ . For the simulation tests, we do not apply any position constraints, as our aim is to solely compare the success rates and the smoothness of the trajectories generated by different methods.

For the assessment of trajectory quality, we calculate the maximum acceleration, average acceleration, and acceleration standard deviation for each dimension (x,y,z, roll, pitch, and yaw) and for each environment condition (25 environments for each seed). Then we calculate the average among dimensions and environments. For example

$$\text{avg-max-lin} = \frac{1}{25} \sum_{i=1}^{25} \frac{a_{x,max}^i + a_{y,max}^i + a_{z,max}^i}{3},$$

TABLE I: Summary of success rates. We use the imitation learning benchmark, RoboMimic (Visual Policy) [12]. We present the average of the maximum success rate (%) across 3 training seeds and 25 different initial environmental conditions (totaling 75 conditions). Results for IBC were sourced from [2] to enable a comparison with conventional methods. The black bold font indicates the highest success rate among all tasks. Notably, for the square task, LeTO achieves a comparable success rate to diffusion policy (bold in green) and surpasses diffusion policy with constraints clipping.

	Can		Square	
	ph	mh	ph	mh
IBC [10]	8	0	3	0
LSTM-GMM [12]	94.6 ± 2.3	94.6 ± 2.3	78.7 ± 6.1	77.3 ± 8.3
LSTM-GMM clipping	90.7 ± 4.6	89.3 ± 2.3	73.3 ± 8.3	70.7 ± 2.3
DiffusionPolicy [2]	<b>100.0 ± 0.0</b>	<b>100.0 ± 0.0</b>	<b>98.7 ± 2.3</b>	<b>90.7 ± 4.6</b>
DiffusionPolicy clipping	98.7 ± 2.3	93.3 ± 4.6	92.0 ± 4.0	82.7 ± 2.3
LeTO	<b>100.0 ± 0.0</b>	<b>100.0 ± 0.0</b>	<b>94.7 ± 4.6</b>	<b>88.0 ± 4.0</b>

TABLE II: Trajectory metrics ( $10^{-2}$ ) of the can-ph task. The results correspond to the results in Table I.

	avg-mean-lin	avg-max-lin	avg-std-lin	avg-mean-rot	avg-max-rot	avg-std-rot	num-of-opt
DiffusionPolicy [2]	8.23 ± 0.70	69.78 ± 2.67	8.39 ± 0.58	<b>1.03 ± 0.12</b>	12.73 ± 0.78	<b>1.29 ± 0.12</b>	2
LSTM-GMM [12]	9.78 ± 3.54	77.49 ± 15.16	10.61 ± 3.48	<b>1.04 ± 0.27</b>	24.58 ± 9.73	2.71 ± 0.26	1
DiffusionPolicy clipping	7.73 ± 0.10	<b>10.00 ± 0.00</b>	<b>3.21 ± 0.06</b>	3.61 ± 0.47	<b>9.94 ± 0.07</b>	2.45 ± 0.08	3
LSTM-GMM clipping	5.61 ± 1.03	<b>10.00 ± 0.00</b>	3.68 ± 0.10	1.16 ± 0.13	<b>9.59 ± 0.14</b>	<b>1.37 ± 0.05</b>	3
LeTO	<b>4.36 ± 0.10</b>	<b>10.00 ± 0.00</b>	<b>3.47 ± 0.03</b>	1.50 ± 0.21	<b>9.78 ± 0.37</b>	1.73 ± 0.30	<b>4</b>

TABLE III: Trajectory metrics ( $10^{-2}$ ) of the can-mh task. The results correspond to the results in Table I.

	avg-mean-lin	avg-max-lin	avg-std-lin	avg-mean-rot	avg-max-rot	avg-std-rot	num-of-opt
DiffusionPolicy [2]	5.97 ± 0.93	64.85 ± 9.04	7.32 ± 0.85	<b>0.60 ± 0.06</b>	10.95 ± 1.16	<b>0.96 ± 0.09</b>	2
LSTM-GMM [12]	6.02 ± 0.78	72.16 ± 1.94	7.41 ± 0.36	0.75 ± 0.08	21.48 ± 9.64	1.57 ± 0.50	0
DiffusionPolicy clipping	7.35 ± 0.14	<b>10.00 ± 0.00</b>	3.30 ± 0.03	2.74 ± 0.19	9.80 ± 0.07	2.26 ± 0.12	1
LSTM-GMM clipping	4.74 ± 0.46	<b>10.00 ± 0.00</b>	3.45 ± 0.10	0.79 ± 0.10	9.16 ± 0.87	1.19 ± 0.43	1
LeTO	<b>2.66 ± 0.68</b>	<b>10.00 ± 0.00</b>	<b>2.60 ± 0.31</b>	0.74 ± 0.22	<b>8.28 ± 1.04</b>	<b>0.98 ± 0.24</b>	<b>5</b>

TABLE IV: Trajectory metrics ( $10^{-2}$ ) of the square-ph task. The results correspond to the results in Table I.

	avg-mean-lin	avg-max-lin	avg-std-lin	avg-mean-rot	avg-max-rot	avg-std-rot	num-of-opt
DiffusionPolicy [2]	8.17 ± 0.78	70.66 ± 4.49	8.65 ± 0.40	<b>0.95 ± 0.11</b>	13.22 ± 0.80	<b>1.32 ± 0.11</b>	2
LSTM-GMM [12]	8.19 ± 2.49	68.75 ± 6.52	8.76 ± 1.82	<b>0.91 ± 0.08</b>	13.81 ± 3.51	<b>1.30 ± 0.24</b>	2
DiffusionPolicy clipping	6.90 ± 0.75	<b>10.00 ± 0.00</b>	<b>3.36 ± 0.06</b>	2.09 ± 0.88	<b>9.09 ± 0.82</b>	1.75 ± 0.59	3
LSTM-GMM clipping	<b>5.11 ± 1.46</b>	<b>10.00 ± 0.00</b>	<b>3.36 ± 0.20</b>	<b>0.98 ± 0.22</b>	<b>9.04 ± 0.54</b>	<b>1.27 ± 0.29</b>	<b>6</b>
LeTO	<b>5.08 ± 0.33</b>	<b>10.00 ± 0.00</b>	<b>3.35 ± 0.03</b>	1.28 ± 0.17	<b>9.24 ± 0.15</b>	<b>1.37 ± 0.08</b>	5

where  $i$  represents the  $i$ -th environment and  $a$  represents acceleration. “lin” here represents linear motion and “rot” represents rotational motion. The remaining matrices can be computed by analogy. Additionally, it is worth noting that the values of the acceleration here are obtained by computing the difference of the normalized velocity. It is directly proportional to the actual acceleration, and this proportionality constant is a fixed value for all experiments. We mark the values within the range of 100% to 110% of the minimum value in each metric as the optimal indicators (bolded), and denote the number of optimal indicators for each method as “num-of-opt”.

In order to investigate the impact of direct action clipping on success rate and trajectory smoothness for baselines, we implement a clipping method. It involves evaluating the difference between the generated action and the previously executed action to determine if it falls within the range of -0.1 to 0.1, which is the same constraints we implement for LeTO. If it exceeds this range, we apply clipping to bring it within this range. This approach constrains acceleration.

We observe that LeTO significantly enhances trajectory smoothness by trajectory optimization while maintaining a consistently high success rate across all simulation tasks. LeTO achieves a success rate comparable to diffusion policy and surpassing LSTM-GMM and IBC. Interestingly, when

applying clipping to constrain the actions generated by the diffusion policy and LSTM-GMM, although this method sometimes increases the smoothness of the trajectory, it results in a reduction in their task success rates.

An intuitive explanation for this phenomenon is that both of these methods do not consider constraints during their training process; they merely fitted human demonstrations. When constraints are imposed on the actions generated by the trained models during deployment, it introduces additional factors that inevitably affect their performance. In contrast, our proposed LeTO, due to its ability to achieve end-to-end trajectory optimization while fitting demonstration data, balance the training objectives of satisfying constraints, smoothing the trajectories, and minimizing errors with demonstrations.

## V. REALWORLD EVALUATION

For real robot experiments, we tackled constraints-critical tasks that demand smooth and safe trajectories, which are Move-the-stack (Fig. 5) and Arrange-chopsticks (Fig. 7). We use SpaceMouse teleoperating the end-effector of the robot manipulator to collect human demonstration data. More details of experiments and results can be seen in the attached video.

TABLE V: Trajectory metrics ( $10^{-2}$ ) of the square-mh task. The results correspond to the results in Table I.

	avg-mean-lin	avg-max-lin	avg-std-lin	avg-mean-rot	avg-max-rot	avg-std-rot	num-of-opt
DiffusionPolicy [2]	$5.42 \pm 0.30$	$60.97 \pm 4.38$	$6.61 \pm 0.44$	<b><math>0.57 \pm 0.08</math></b>	$13.41 \pm 3.45$	$1.11 \pm 0.26$	1
LSTM-GMM [12]	$5.37 \pm 0.66$	$54.43 \pm 6.99$	$6.28 \pm 1.00$	$0.64 \pm 0.08$	$13.31 \pm 2.66$	$1.04 \pm 0.22$	0
DiffusionPolicy clipping	$7.04 \pm 0.42$	<b><math>10.00 \pm 0.00</math></b>	$3.35 \pm 0.06$	$2.41 \pm 0.50$	$9.46 \pm 0.34$	$2.04 \pm 0.36$	1
LSTM-GMM clipping	$3.81 \pm 0.44$	<b><math>10.00 \pm 0.00</math></b>	$3.07 \pm 0.13$	<b><math>0.63 \pm 0.04</math></b>	<b><math>7.80 \pm 0.23</math></b>	<b><math>0.85 \pm 0.04</math></b>	<b>4</b>
LeTO	<b><math>3.08 \pm 0.04</math></b>	<b><math>10.00 \pm 0.00</math></b>	<b><math>2.70 \pm 0.01</math></b>	$0.91 \pm 0.06$	<b><math>8.18 \pm 0.07</math></b>	$1.09 \pm 0.07$	<b>4</b>

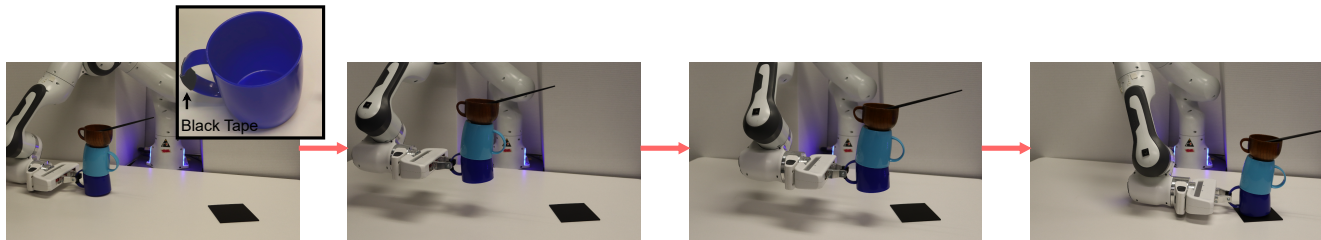


Fig. 5: Move-the-stack task. The robot grasps a set of stacked objects, smoothly transport them, and ultimately place them onto a black board, ensuring none of the stacked objects fall off. The black tape is for marking a consistent grasping position.

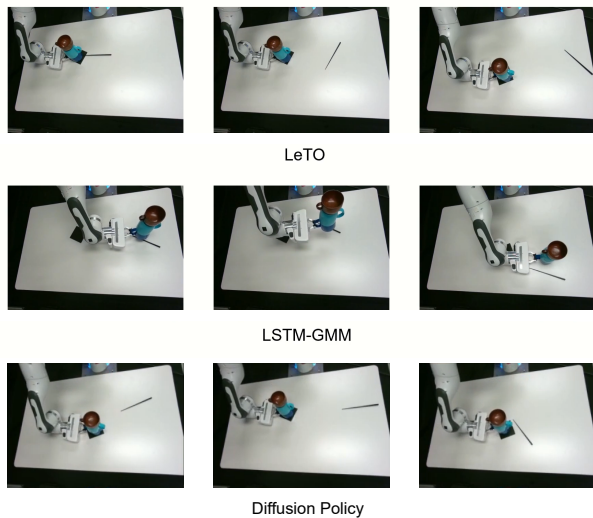


Fig. 6: When chopsticks fall, which is a type of OOD data, both the diffusion policy and LeTO can still move the stacked cups and place them on the black board. In contrast, LSTM-GMM often exhibits erroneous behaviors, such as moving to incorrect locations or acting erratically.

TABLE VI: Metrics for evaluating the Move-the-stack task. “acc-peak” represents the highest acceleration achieved in any of the test trials while “avg-acc-mean/max/std” are the average of mean/max/std values across all test trials.

	avg-acc-mean/max/std	succ-rate	acc-peak
LSTM-GMM	$0.053/0.480/0.081$	4/20	0.647
DiffusionPolicy	$0.037/0.336/0.055$	4/20	0.721
LeTO	$0.037/0.219/0.042$	<b>13/20</b>	<b>0.250</b>

### A. Move-the-stack

The objective of the “Move-the-stack” task is that the robot grasps a set of stacked objects, smoothly transport them, and ultimately place them onto a black board, ensuring none of the stacked objects fall off. The initial position of the robot and the black board are randomized. The policy inputs end-effector positions and images from a third-person perspective camera, and controls the end-effector position. We introduce velocity constraint  $[-1,1]$  and acceleration con-

TABLE VII: Metrics for evaluating the Arrange-chopsticks task. “contact-peak” represents the highest contact force achieved in any of the test trials while “avg-contact-max” is the average of max contact forces across all test trials.

	avg-contact-max	contact-peak	succ-rate
LSTM-GMM	13.2 N	27.3 N	0/20
DiffusionPolicy	13.9 N	24.8 N	<b>18/20</b>
LeTO	<b>11.7 N</b>	<b>16.1 N</b>	<b>17/20</b>

straint  $[-0.25,0.25]$  for LeTO. Notably, while we did not place chopsticks on top during human demonstration collection, a chopstick was added atop the stacked cups during policy rollout.

For imitation learning algorithms, the task is challenging because: 1) The policy needs to generate very smooth trajectories. Any roughness in the trajectory can lead to vibrations at the robot’s end-effector, causing the cups to shake. This vibration can accumulate and lead to the chopstick dropping. 2) Since a chopstick is introduced during policy rollout, this out-of-distribution (OOD) observation adds greater uncertainty to the network’s input. This uncertainty may make the network’s output jerkier, resulting in a poorer quality trajectory.

The results are shown in Table VI. From the results, LeTO excels in terms of trajectory smoothness and, correspondingly, also boasts the highest success rate. This demonstrates that due to the presence of end-to-end trajectory optimization, LeTO can robustly maintain its effectiveness even when facing OOD data. Another point worth noting is that when chopsticks fall (which is also a type of OOD data), both the diffusion policy and LeTO can still move the stacked cups and place them on the black board. In contrast, LSTM-GMM often exhibits erroneous behaviors, such as moving to incorrect locations or acting erratically (see Fig. 6 and the attached video). This showcases the robustness of LeTO and the diffusion policy.

### B. Arrange-chopsticks

The objective of the “Arrange-chopsticks” task is to pick up randomly placed two chopsticks and arrange them neatly on a bowl. The policy inputs end-effector poses and images

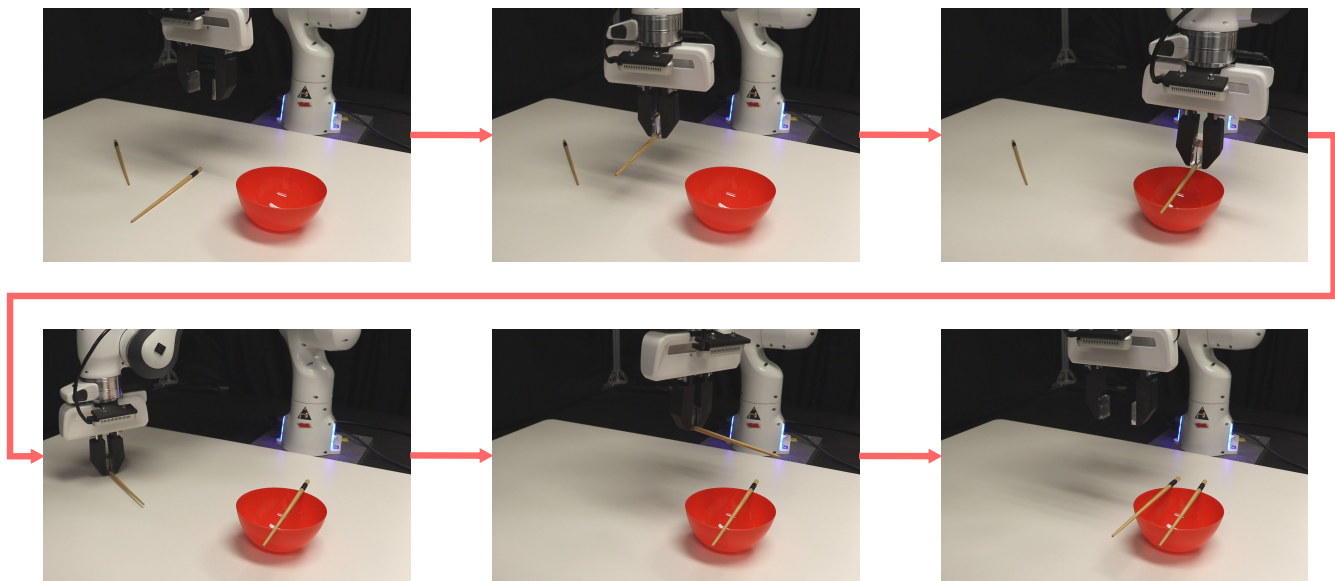


Fig. 7: Arrange-chopsticks task. The robot picks up randomly placed two chopsticks and arrange them neatly on a bowl.

from two cameras, a third-person perspective camera and a wrist-mounted camera, and controls the end-effector position, yaw angle, and grasping.

The challenges of this task include: 1. It is a relative long-horizon task, requiring the policy to have the capability to represent complex tasks. 2. Due to the slender nature of chopsticks, there is a high risk of the robot making forceful contact with the table when attempting to grasp them. For the sake of hardware safety, such collisions should be minimized as much as possible.

We introduce both position, velocity, and acceleration constraints for LeTO. During the demonstration, the lowest position of the robot’s end-effector on the z-axis was recorded at 0.0501 m. We have opted for 0.0475 m as the z-axis positional constraint within the LeTO framework. This choice is made with the task’s completion in mind, where the goal is not to prevent any contact between the robot’s end-effector and the table surface, but rather to allow for the slightest possible contact that still enables the picking up of slender chopsticks.

The results are shown in Table VII. Both LeTO and diffusion policy have high success rate, but the contact forces in LeTO tests are significantly smaller.

## VI. DISCUSSION AND FUTURE WORK

In this paper, we present LeTO, a framework for learning constrained visuomotor policy with differentiable trajectory optimization. By balancing the objective of minimizing errors with the need to satisfy trajectory constraints, LeTO allows for deployment in tasks where safety and reliability are paramount.

### A. Hyperparameter, Training Time, and Training Stability

Regarding LeTO, its core neural network comprises CNN+LSTM, which is identical to the architecture of the

TABLE VIII: The training time for 20 epochs on the square ph task with a batch size of 64, conducted on a single GeForce RTX 3080. The hyperparameters for diffusion policy and LSTM-GMM are adopted from the default parameters reported in [2], [12], respectively. For the hyperparameters of LeTO, please refer to our open-source code.

Policy	LSTM-GMM	DiffusionPolicy	LeTO
Training Time	2.90 hours	0.92 hours	7.25 hours

basic imitation learning method BC-RNN. Therefore, we believe the discussion of hyperparameters of LeTO’s core network can refer to the discussion for BC-RNN in [12].

Concerning the hyperparameters of the DTO layer, since it comes from model-based formulation, it is possible to intuitively summarize how to select effective hyperparameters:

1. As shown in Remark 1, the optimization problem of the DTO layer is always feasible during training, given that the positions (and orientations) in the dataset meet the set position constraints. The consistent feasibility of the DTO layer ensures training stability, which is evident from the training logs of LeTO available in our open-source code.

2. In terms of constraints for acceleration and velocity, it is important to avoid overly small constraints. This could lead to a significant discrepancy between the generated trajectory and the dataset’s trajectory, adversely affecting model performance even with stable training. In our simulation experiments, LeTO trained at a maximum acceleration of 0.1 (normalized value) shows high performance, but setting it to 0.01 (normalized value) may result in worse outcomes. By analogy, the same consideration applies to the smoothing weight.

Table VIII compares the training times of LSTM-GMM, diffusion policy, and LeTO. We acknowledge that one limitation of LeTO is the computational overhead introduced by the differentiable optimization layer. Future work could look into improving the computational efficiency of the differentiable optimization process, potentially through the

use of more efficient solvers or by learning approximations of the optimization layer.

### B. LeTO in Low-data and High-data Regimes

We would like to highlight that networks with the training objective of minimizing the errors for fitting human demonstrated actions can readily incorporate our proposed DTO layer at the head. This suggests that for scalability, one could consider designing a LeTO variant with transformer, enhancing the model’s capability to scale to large datasets. However, the time and cost involved in training could still be a limiting factor. Therefore, future research focused on accelerating differentiable optimization is pivotal for scalability.

Furthermore, exploring policies that excel in low-data regimes based on differentiable optimization layers is an intriguing research direction. By constructing differentiable optimization layers using prior knowledge of the model, policy may reduce reliance on data.

### C. LeTO in Reinforcement Learning

Due to the differentiability, the DTO layer can be designed to be integrated into the robot learning pipelines, enabling end-to-end optimization and inference. This opens up the possibility of extending LeTO to reinforcement learning, offering a promising future research direction. By integrating differentiable trajectory optimization with reinforcement learning, it is possible to ensure that the generated actions comply with the designed constraints, thereby significantly enhancing the safety and interpretability of the policy.

### D. LeTO in High-safety Scenarios

The safe and constraint-controlled output form of LeTO holds significant potential in robot learning scenarios where safety is of utmost importance, such as in human-robot interaction and surgical robotics. Investigating the application of LeTO, or more broadly, robot policies that integrate differential optimization in these settings, represents a highly interesting and promising research direction.

## REFERENCES

- [1] D. A. Pomerleau, “Alvin: An autonomous land vehicle in a neural network,” *Advances in neural information processing systems*, vol. 1, 1988.
- [2] C. Chi, S. Feng, Y. Du, Z. Xu, E. Cousineau, B. Burchfiel, and S. Song, “Diffusion policy: Visuomotor policy learning via action diffusion,” in *Proceedings of Robotics: Science and Systems (RSS)*, 2023.
- [3] C. Chi, Z. Xu, C. Pan, E. Cousineau, B. Burchfiel, S. Feng, R. Tedrake, and S. Song, “Universal manipulation interface: In-the-wild robot teaching without in-the-wild robots,” *arXiv preprint arXiv:2402.10329*, 2024.
- [4] T. Z. Zhao, V. Kumar, S. Levine, and C. Finn, “Learning fine-grained bimanual manipulation with low-cost hardware,” *arXiv preprint arXiv:2304.13705*, 2023.
- [5] Z. Fu, T. Z. Zhao, and C. Finn, “Mobile aloha: Learning bimanual mobile manipulation with low-cost whole-body teleoperation,” *arXiv preprint arXiv:2401.02117*, 2024.
- [6] Y. Zhu, A. Joshi, P. Stone, and Y. Zhu, “Viola: Imitation learning for vision-based manipulation with object proposal priors,” *arXiv preprint arXiv:2210.11339*, 2022.
- [7] C. Wang, L. Fan, J. Sun, R. Zhang, L. Fei-Fei, D. Xu, Y. Zhu, and A. Anandkumar, “Mimicplay: Long-horizon imitation learning by watching human play,” *arXiv preprint arXiv:2302.12422*, 2023.
- [8] L. Wang, J. Zhao, Y. Du, E. H. Adelson, and R. Tedrake, “Poco: Policy composition from and for heterogeneous robot learning,” *arXiv preprint arXiv:2402.02511*, 2024.
- [9] D. Jarrett, I. Bica, and M. van der Schaar, “Strictly batch imitation learning by energy-based distribution matching,” *Advances in Neural Information Processing Systems*, vol. 33, pp. 7354–7365, 2020.
- [10] P. Florence, C. Lynch, A. Zeng, O. A. Ramirez, A. Wahid, L. Downs, A. Wong, J. Lee, I. Mordatch, and J. Tompson, “Implicit behavioral cloning,” in *Conference on Robot Learning*. PMLR, 2022, pp. 158–168.
- [11] C. Chi, B. Burchfiel, E. Cousineau, S. Feng, and S. Song, “Iterative Residual Policy: for goal-conditioned dynamic manipulation of deformable objects,” in *in Proc. of Robot.: Sci. and Syst.*, 2022.
- [12] A. Mandlekar, D. Xu, J. Wong, S. Nasiriany, C. Wang, R. Kulkarni, L. Fei-Fei, S. Savarese, Y. Zhu, and R. Martín-Martín, “What matters in learning from offline human demonstrations for robot manipulation,” in *Proc. Conf. Robot Learn.*, 2022, pp. 1678–1690.
- [13] M. Zucker, N. Ratliff, A. D. Dragan, M. Pivtoraiko, M. Klingensmith, C. M. Dellin, J. A. Bagnell, and S. S. Srinivasa, “Chomp: Covariant hamiltonian optimization for motion planning,” *The International journal of robotics research*, vol. 32, no. 9-10, pp. 1164–1193, 2013.
- [14] J. Schulman, Y. Duan, J. Ho, A. Lee, I. Awwal, H. Bradlow, J. Pan, S. Patil, K. Goldberg, and P. Abbeel, “Motion planning with sequential convex optimization and convex collision checking,” *The International Journal of Robotics Research*, vol. 33, no. 9, pp. 1251–1270, 2014.
- [15] D. Mellinger and V. Kumar, “Minimum snap trajectory generation and control for quadrotors,” in *2011 IEEE international conference on robotics and automation*. IEEE, 2011, pp. 2520–2525.
- [16] X. Zhang, A. Liniger, and F. Borrelli, “Optimization-based collision avoidance,” *IEEE Transactions on Control Systems Technology*, vol. 29, no. 3, pp. 972–983, 2020.
- [17] T. Zhang, Z. McCarthy, O. Jow, D. Lee, X. Chen, K. Goldberg, and P. Abbeel, “Deep imitation learning for complex manipulation tasks from virtual reality teleoperation,” in *2018 IEEE International Conference on Robotics and Automation (ICRA)*. IEEE, 2018, pp. 5628–5635.
- [18] P. Florence, L. Manuelli, and R. Tedrake, “Self-supervised correspondence in visuomotor policy learning,” *IEEE Robotics and Automation Letters*, vol. 5, no. 2, pp. 492–499, 2019.
- [19] M. Bojarski, D. Del Testa, D. Dworakowski, B. Firner, B. Flepp, P. Goyal, L. D. Jackel, M. Monfort, U. Muller, J. Zhang *et al.*, “End to end learning for self-driving cars,” *arXiv preprint arXiv:1604.07316*, 2016.
- [20] S. Ross, G. Gordon, and D. Bagnell, “A reduction of imitation learning and structured prediction to no-regret online learning,” in *Proceedings of the fourteenth international conference on artificial intelligence and statistics*. JMLR Workshop and Conference Proceedings, 2011, pp. 627–635.
- [21] R. Rahmatizadeh, P. Abolghasemi, L. Bölöni, and S. Levine, “Vision-based multi-task manipulation for inexpensive robots using end-to-end learning from demonstration,” in *2018 IEEE international conference on robotics and automation (ICRA)*. IEEE, 2018, pp. 3758–3765.
- [22] J. Wu, X. Sun, A. Zeng, S. Song, J. Lee, S. Rusinkiewicz, and T. Funkhouser, “Spatial action maps for mobile manipulation,” *arXiv preprint arXiv:2004.09141*, 2020.
- [23] A. Zeng, P. Florence, J. Tompson, S. Welker, J. Chien, M. Attarian, T. Armstrong, I. Krasin, D. Duong, V. Sindhwani *et al.*, “Transporter networks: Rearranging the visual world for robotic manipulation,” in *Conference on Robot Learning*. PMLR, 2021, pp. 726–747.
- [24] Y. Avigal, L. Berscheid, T. Asfour, T. Kröger, and K. Goldberg, “Speedfolding: Learning efficient bimanual folding of garments,” in *2022 IEEE/RSJ International Conference on Intelligent Robots and Systems (IROS)*. IEEE, 2022, pp. 1–8.
- [25] N. M. Shafiqullah, Z. Cui, A. A. Altanzaya, and L. Pinto, “Behavior transformers: Cloning  $k$  modes with one stone,” *Advances in neural information processing systems*, vol. 35, pp. 22955–22968, 2022.
- [26] S. Pfrommer, M. Halm, and M. Posa, “ContactNets: Learning Discontinuous Contact Dynamics with Smooth, Implicit Representations,” in *The Conference on Robot Learning (CoRL)*, 2020. [Online]. Available: <https://proceedings.mlr.press/v155/pfrommer21a.html>
- [27] B. Bianchini, M. Halm, N. Matni, and M. Posa, “Generalization bounded implicit learning of nearly discontinuous functions,”

- in *Proceedings of The 4th Annual Learning for Dynamics and Control Conference (LADC)*, ser. Proceedings of Machine Learning Research, R. Firoozi, N. Mehr, E. Yel, R. Antonova, J. Bohg, M. Schwager, and M. Kochenderfer, Eds., vol. 168. PMLR, 23–24 Jun 2022, pp. 1112–1124. [Online]. Available: <https://proceedings.mlr.press/v168/bianchini22a.html>
- [28] B. Amos, I. Jimenez, J. Sacks, B. Boots, and J. Z. Kolter, “Differentiable mpc for end-to-end planning and control,” *Advances in neural information processing systems*, vol. 31, 2018.
- [29] M. Retchin, B. Amos, S. Brunton, and S. Song, “Koopman constrained policy optimization: A koopman operator theoretic method for differentiable optimal control in robotics,” in *ICML 2023 Workshop on Differentiable Almost Everything: Differentiable Relaxations, Algorithms, Operators, and Simulators*, 2023. [Online]. Available: <https://openreview.net/forum?id=3W7vPqWCeM>
- [30] Z. Xu and Y. She, “Letac-mpc: Learning model predictive control for tactile-reactive grasping,” *arXiv preprint arXiv:2403.04934*, 2024.
- [31] W. Xiao, R. Hasani, X. Li, and D. Rus, “Barriernet: A safety-guaranteed layer for neural networks,” *arXiv preprint arXiv:2111.11277*, 2021.
- [32] C. Diehl, J. Adamek, M. Krüger, F. Hoffmann, and T. Bertram, “Differentiable constrained imitation learning for robot motion planning and control,” *arXiv preprint arXiv:2210.11796*, 2022.
- [33] P. Karkus, B. Ivanovic, S. Mannor, and M. Pavone, “Diffstack: A differentiable and modular control stack for autonomous vehicles,” in *Conference on Robot Learning*. PMLR, 2023, pp. 2170–2180.
- [34] W. Wan, Y. Wang, Z. Erickson, and D. Held, “Difftop: Differentiable trajectory optimization for deep reinforcement and imitation learning,” *arXiv preprint arXiv:2402.05421*, 2024.
- [35] N. D. Ratliff, J. Issac, D. Kappler, S. Birchfield, and D. Fox, “Riemannian motion policies,” *arXiv preprint arXiv:1801.02854*, 2018.
- [36] A. Li, C.-A. Cheng, M. A. Rana, M. Xie, K. Van Wyk, N. Ratliff, and B. Boots, “Rmp2: A structured composable policy class for robot learning,” *arXiv preprint arXiv:2103.05922*, 2021.
- [37] C.-A. Cheng, M. Mukadam, J. Issac, S. Birchfield, D. Fox, B. Boots, and N. Ratliff, “Rmp flow: A computational graph for automatic motion policy generation,” in *Algorithmic Foundations of Robotics XIII: Proceedings of the 13th Workshop on the Algorithmic Foundations of Robotics 13*. Springer, 2020, pp. 441–457.
- [38] A. Mandlekar, D. Xu, R. Martín-Martín, S. Savarese, and L. Fei-Fei, “Learning to generalize across long-horizon tasks from human demonstrations,” *arXiv preprint arXiv:2003.06085*, 2020.
- [39] A. Mandlekar, F. Ramos, B. Boots, S. Savarese, L. Fei-Fei, A. Garg, and D. Fox, “Iris: Implicit reinforcement without interaction at scale for learning control from offline robot manipulation data,” in *2020 IEEE International Conference on Robotics and Automation (ICRA)*. IEEE, 2020, pp. 4414–4420.
- [40] B. Amos and J. Z. Kolter, “OptNet: Differentiable optimization as a layer in neural networks,” in *Proc. 34th Int. Conf. Mach. Learn.*, 2017, pp. 136–145.
- [41] S. Boyd, S. P. Boyd, and L. Vandenberghe, *Convex optimization*. Cambridge university press, 2004.